Nano Energy 65 (2019) 104042

Contents lists available at ScienceDirect

Nano Energy

journal homepage: www.elsevier.com/locate/nanoen

Full paper

Face-to-face intercrossed ZnO nanorod arrays with extensive NR-NR homojunctions for a highly sensitive and self-powered ultraviolet photodetector

Changsong Chen[a,c], Baofa Hu[a], Zhen Wang[a], Xueqin Lv[a], Chunquan Zhang[a], Binbin Chen[a], Haisheng San[a,b,*], Werner Hofmann[a,c]

[a] Pen-Tung Sah Institute of Micro-Nano Science and Technology, Xiamen University, Xiamen, 361005, China
[b] Shenzhen Research Institute of Xiamen University, Shenzhen, 518000, China
[c] Institute of Solid State Physics, Technical University of Berlin, Berlin, 10623, Germany

ARTICLE INFO

Keywords:
UV photodetection
Self-powered device
ZnO nanorod arrays
Face-to-face hybrid
ZnO nanostructure homojunction

ABSTRACT

A self-powering ultraviolet photodetector (UVPD) that effectively utilizes UV energy in an easy-to-implement way is an attractive alternative for the UV optical sensing and communication. Here we report a novel self-powered UVPD based on a face-to-face hybrid ZnO nanorod arrays (ZNRAs) nanostructure. Large-area free-standing ZNRAs have been grown on indium tin oxide (ITO) conductive glass and Ti substrates through a hydrothermal method. Different geometric dimension of ZNRAs/ITO and ZNRAs/Ti structures were designed to pair hybrid each other for achieving the optimum photoelectric performance. Experimentally, it is found that the optimum UVPD based on face-to-face hybrid ITO/*l*-ZNRAs/*l*-ZNRAs/Ti structure exhibits an enhancement of '1 + 1 > 2' in photoelectric conversion without applying any external DC voltage when compared with single-face ZNRAs-based UVPDs, and the optimum UVPD demonstrates a responsivity of 2.45 mA W^{-1} and on/off current ratio of 6.6×10^5 under a UV irradiation of 3.06 μW cm^{-2} as well as a high durability with a cyclic balance of no less than 93.5% in a 4250-s on/off irradiation. The generation of self-power and the high photoelectric performance of face-to-face hybrid ZNRAs-based UVPDs are associated to the Schottky junctions in ITO/ZnO interface as well as the extensive ZnO nanorod-nanorod homojunction.

1. Introduction

Ultraviolet photodetectors (UVPDs) with high photoresponse and long-term durability are highly desirable in various practical applications, such as flame alarm, early missile plume detection, and secure space communication [1–4]. UVPDs based on photoconductive response commonly utilize external DC voltage to separate the photo-induced electron-hole pairs (EHPs) for photocurrent test, which are not best choice for the sensing applications in remote and inaccessible locations where the maintain-free power sources are usually demanded. A good strategy is to use the self-powered device capable of harvesting energy from the surrounding environment to power its own electronic devices and circuits. To meet continuous self-powered operations, the photodetectors based on photovoltaic effect are able to be operated without the demand of external bias [5–7]. Owing to the effective presence of built-in potential in the functional heterojunction of photodetectors, the photo-induced EHPs can be separated and transported to contribute to the generation of photocurrent of devices without external bias.

Zinc oxide (ZnO), a wide direct bandgap semiconducting oxide material (bandgap = 3.37 eV), has been extensively studied toward realizing high-performance UVPDs due to its excellent performance in UV photoconductivity and electron mobility [8]. Especially, one-dimensional (1-D) ZnO nanostructures have attracted tremendous attention because of its unique photoelectronic and chemical properties, surface effect and quantum-size effect. Furthermore, three-dimensional (3-D) ZnO nanostructure, e.g. free-standing ZnO nanorod arrays (ZNRAs) [9] and ZnO nanotube arrays [10], can be self-assembled from 1-D ZnO nanostructures using low-cost solution-synthesized method on a vast variety of substrates to provide multiple strategies for surface functionalization and carrier transport [11,12]. In the past few years, there has been an increasing interest in 1-D ZnO-based self-powered UVPDs and their various applications [13–15]. However, the pure 1-D ZnO nanostructure arrays generally have their own shortcomings, e.g.

* Corresponding author. Pen-Tung Sah Institute of Micro-Nano Science and Technology, Xiamen University, Xiamen, 361005, China.
E-mail address: sanhs@xmu.edu.cn (H. San).

https://doi.org/10.1016/j.nanoen.2019.104042
Received 13 July 2019; Received in revised form 18 August 2019; Accepted 19 August 2019
Available online 22 August 2019

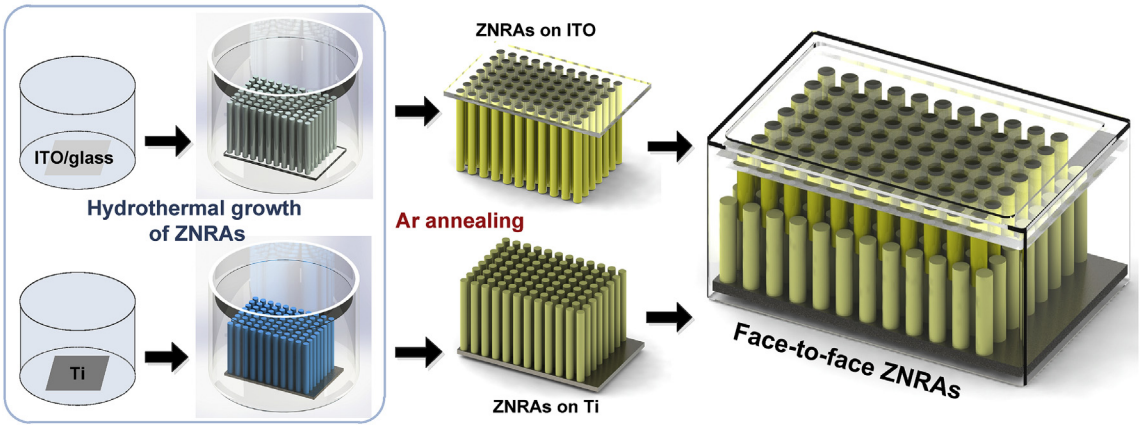

Fig. 1. Schematic illustration of fabrication processes of UVPDs based on face-to-face hybrid ZNRAs-based nanostructure.

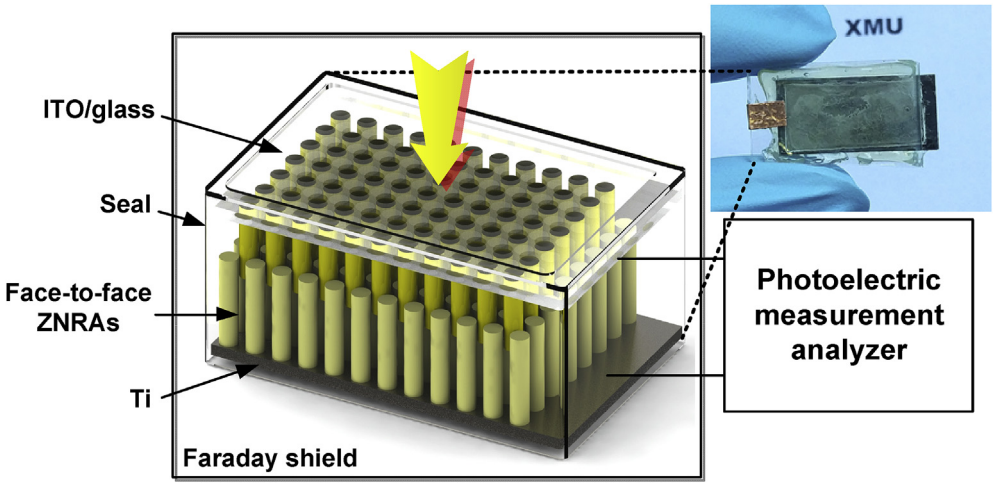

Fig. 2. Schematic structure of UVPDs based on face-to-face hybrid ZNRAs-based nanostructure and the photograph of the actual photodetector.

the lack of built-in potential for EHPs separating and high interface resistance when contacting with a planar electrode. Interface engineering is an effective way to improve the device performance by optimizing the interfacial contact, energy band structure, barrier height, depletion region, and surface defect states [16,17]. Recently it has become a promising method to modify the interfacial physical and chemical properties at the surface of ZnO nanostructures utilizing the piezotronic effect, which is the coupling of semiconductor properties and piezoelectric effects [15]. Researchers have engineered the valid sensitization and separation mechanisms in ZnO-based photodetectors by means of hybridizing ZnO with other materials, e.g. carbon allotropes [18], noble metal [19], metal compounds [20] and auxiliary semiconductors [12]. However, these 1-D ZnO-based composite nanostructures generally rely on the complicated preparation processes at high cost, showing limited performances in photoresponsivity, reproducibility and long-term durability [12].

In this work, a self-powered UV photodetector is presented based on a novel face-to-face hybrid ZNRAs nanostructure. The unique 3-D nanostructure was assembled using two kinds of free-standing ZNRAs nanostructures to face-to-face intercross together without extra heterogeneous modification. Owing to the formation of a large surface-to-volume ratio of nanorod-nanorod (NR-NR) homojunction with built-in potential perpendicular to nanorod surface, the novel nanostructure enables a beneficial effect in the fast transportation and effective separation of the photo-induced EHPs. As a result, the cyclic photoresponse and long-term durability of the photodetectors are significantly enhanced. Although UVPDs based on ZnO nanostructures have been extensively investigated, there were few reports about the self-powered UVPDs based on such unique face-to-face hybrid ZNRAs nanostructures.

2. Materials and methods

2.1. Synthesis of materials and fabrication of devices

The fabrication processes of the UVPDs based on face-to-face hybrid ZNRAs nanostructure are schematically illustrated in Fig. 1. The free-standing ZNRAs were prepared on indium tin oxide (ITO)/glass and titanium (Ti) foil using a facile hydrothermal method. Before the hydrothermal treatment, the ITO/glass substrate and Ti foils (99.9% purity) were cut into appropriate size (ITO/glass, 15 mm × 22 mm × 1.0 mm; Ti, 10 mm × 20 mm × 0.2 mm) and then were degreased and cleaned using acetone, ethanol, and deionized water in ultrasonic bath for 15 min, respectively. After drying, the Scotch tape was used to protect the backside of the Ti substrates. The colloid seed solution was prepared by dissolving zinc acetate [$Zn(CH_3COO)_2{\cdot}2H_2O$] in ethanol with a concentration of 0.05 M. Several drops of colloid seed solution were applied onto a cleaned substrate to cover the entire substrate surface. The substrate was dried at room temperature and then annealed at 300 °C in air for 30 min. The precursor solution was prepared by dissolving 0.02 M Polyethyleneimine (PEI), 0.05 M Zinc nitrate hexahydrate [$Zn(NO_3)_2{\cdot}6H_2O$], 0.05 M hexamethylenetetramine ($(CH_2)_6N_4$, HMTA) in deionized water. In order to fabricate short ZNRAs (e.g. *s*-ZNRAs/Ti and *s*-ZNRAs/ITO) and long

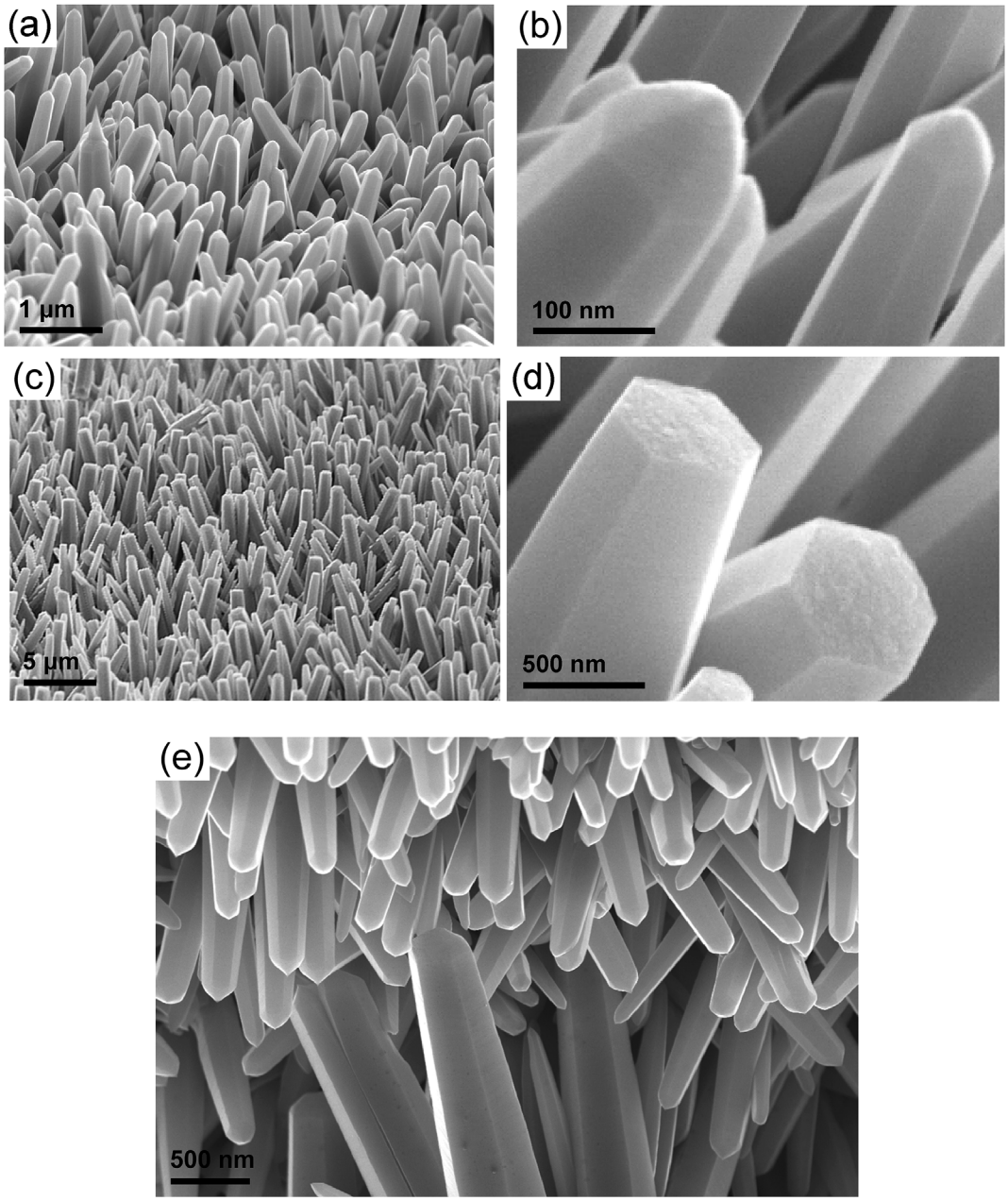

Fig. 3. SEM images of (a) *s*-ZNRAs and (c) *l*-ZNRAs and the partial enlarged images of (b) *s*-ZNRAs and (d) *l*-ZNRAs; (e) SEM images of face-to-face hybrid *s*-ZNRAs/*l*-ZNRAs nanostructure.

ZNRAs (e.g. *l*-ZNRAs/Ti and *l*-ZNRAs/ITO), the temperature of hydrothermal treatment was controlled to 95 °C for 1 h and 5 h, respectively. Next, the as-grown ZNRAs/ITO and ZNRAs/Ti were cleaned by deionized water and annealed in Ar atmosphere at 400 °C for 2 h.

The ZNRAs/ITO and ZNRAs/Ti structures were assembled together in a face-to-face way to form a hybrid device (ITO/ZNRAs/ZNRAs/Ti) by a controllable cantilever system to guarantee the consistence of pressure and overlap distance from sample to sample within each batch. The upper and lower pressure plates in cantilever are controlled to mechanically assemble the ZNRAs/ITO and ZNRAs/Ti sample together with the determined height. Furthermore, the assembled devices were sealed using hot glue (ethylene-vinyl acetate copolymer, EVA) at the device edges to prevent physical and chemical damage, as illustrated in Fig. 1. For a comparative study, four kinds of ZNRAs nanostructures, e.g. *s*-ZNRAs/Ti, *s*-ZNRAs/ITO, *l*-ZNRAs/Ti, and *l*-ZNRAs/ITO, were paired up to fabricate the face-to-face ZNRAs-based UVPDs (see in Fig. S1 in the supporting information). For performing a comparison with the face-to-face ZNRAs-based UVPDs, the single-face ZNRAs UVPDs were also fabricated through assembling *l*-ZNRAs/ITO and *l*-ZNRAs/Ti with bare Ti foil and bare ITO/glass, respectively. The active optical areas of all of devices are 1.0 cm^2. In order to ensure success of device fabrication, same three devices were fabricated in each batch. The same batch of ZNRAs was fabricated with stable process parameters. The repeatability of experimental results has been verified and confirmed by above consistent fabrications and measurements of three devices in each batch.

2.2. Materials characterization and device measurements

The morphology and size of ZNRAs samples were characterized by field emission scanning electron microscopy (FESEM, ZEISS microscope, Germany). The crystal structures of ZNRAs samples were

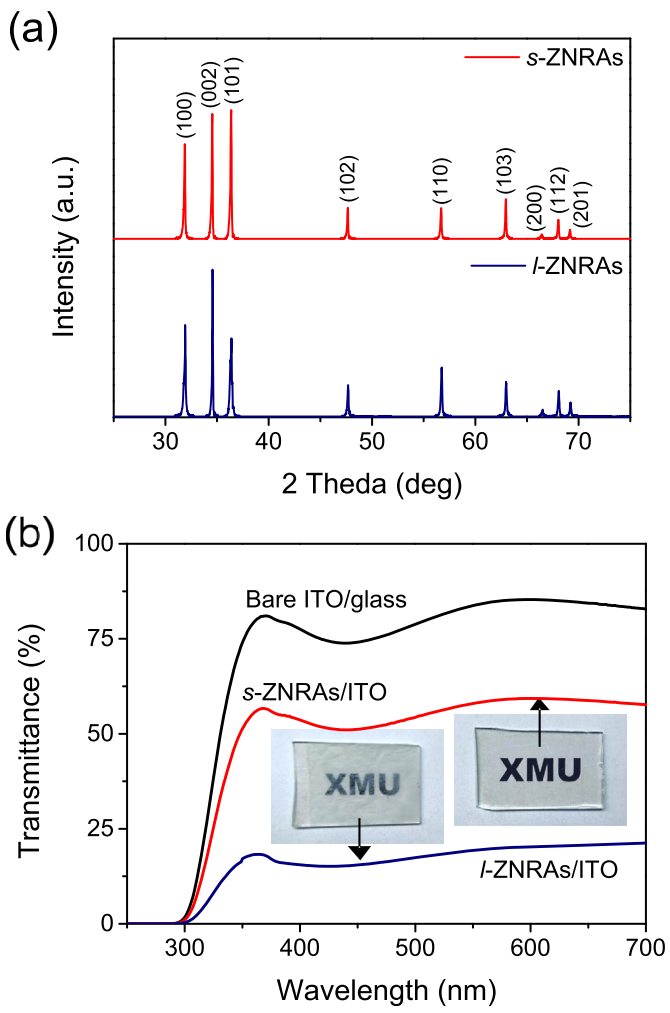

Fig. 4. (a) XRD spectra and (b) UV–Vis transmittance spectra of 1-h grown *s*-ZNRAs and 5-h grown *s*-ZNRAs on ITO substrates.

characterized by X-ray diffraction analysis (XRD, Rigaku Ultima IV, Japan). The Ultraviolet–visible light (UV–Vis) absorption and transmittance spectral measurements of ZNRAs samples were performed using a UV–Vis spectrophotometer (Cary 5000, USA). The photoresponse properties of the fabricated UVPDs were measured using an electrochemical workstation (Chenhua CHI660E, China) under dark and room temperature in a Faraday cage as shown in Fig. 2. A 3.08W UV lamp (NICHIA NCSU033B, Japan) was used as the UV irradiation source with tunable direct current power supply (Agilent E3631A, USA). In the cyclic photoresponse test, the UV light was modulated by a function waveform generator (Agilent 33250A, USA).

3. Results and discussion

As shown in Fig. 3, the SEM images of the ZNRAs samples demonstrate a high surface-to-volume ratio, well-aligned orientation, and hexagonal morphology feature. For the *s*-ZNRAs nanostructure, the nanorods are about 0.8–1.0 μm in length and 150–200 nm in diameter (see Fig. 3(a)–(b)). For the *l*-ZNRAs nanostructure, the nanorods are about 4.0–5.0 μm in length and 700–800 nm in diameter (see Fig. 3(c)–(d)). Fig. 3(e) and Fig. S2 shows the SEM image of the face-to-face hybrid *s*-ZNRAs/*l*-ZNRAs nanostructure. It can be seen that up-side of *s*-ZNRAs intercross with down-side of *l*-ZNRAs in a teeth-to-teeth way. As a result, a high surface-to-volume ratio of NR-NR interface is created along the length direction of nanorods through a fully surface physical contact among ZnO nanorods.

It is found that from Fig. 3(b), a steeple-top with the crystal facet of $\{10\bar{1}1\}$ is observed on the top ends of the 1-h grown *s*-ZNRAs nanostructure, whereas the steeple-top is changed into flat-top when the hydrothermal growth time is increased to 5 h to form the *l*-ZNRAs nanostructure, as shown in Fig. 3(d). The typical 2θ peaks at 34.45° and 36.34° as shown in Fig. 4(a) were well indexed as the (002) and (101) planes of ZnO (JCPDS card No. 36–1451), respectively. The peak height ratio between (002) and (101) peak increases with growth time, indicating that the growth direction of ZnO nanorods prefer to their *c*-axis nearly normal to the substrate with the increase of growth time. Fig. 4(b) shows a comparison of UV–Vis transmittance spectra of bare ITO substrate, *s*-ZNRAs/ITO and *l*-ZNRAs/ITO samples. It is found that all samples have a strong absorption for UV waveband, which is line with the optical properties of wide band-gap semiconductor ZnO and ITO. Furthermore, in comparison with the average 75% of transmittance of ITO substrate in visible waveband, the average transmittance is less than 50% for *s*-ZNRAs/ITO and 25% for *l*-ZNRAs/ITO. This can be explained by the light scattering effect of nanorods arrays; that is to say, the longer the length of nanorods are, the more the dissipation of light energy in nanorod array is and thus the more the harvesting and absorbing of light energy are.

In order to investigate photoelectric properties of different nanostructure ZNRAs-based devices, we performed a comparative study among the face-to-face hybrid ZNRAs-based device (ITO/*s*-ZNRAs/*l*-ZNRAs/Ti) and other two single-face ZNRAs-based devices (bare ITO/*l*-ZNRAs/Ti and ITO/*l*-ZNRAs/bare Ti). The schematic structures of contrast devices are shown in Fig. 5(a). Fig. 5(b) shows the UV–Vis absorption spectra of the three kinds of devices, in which there is no significant absorption difference in UV range. Whereas, the face-to-face hybrid device exhibits a much better *I–V* response under UV irradiation, which can be determined by the curve slope when compared with other two devices, as shown in Fig. 5(c). The typical differential conductance spectra of these devices are presented in Fig. 5(d). Under an UV irradiation with intensity of 2.90 mW cm^{-2}, the face-to-face hybrid device shows a 59.4% and a 621% enhancement in photo-conductance under zero-bias point as compared with the devices based on bare ITO/*l*-ZNRAs/Ti and ITO/*l*-ZNRAs/bare Ti, respectively. Fig. 5(e) exhibits a comparison of time-dependent photoresponse properties of above three kinds of devices. It can be seen that the face-to-face hybrid device exhibits uniform and repeatable photocurrent responses with the maximum current density of 5.57 μA cm^{-2}, showing a 300%–400% enhancement in photocurrent at zero-bias point as compared with the devices based on bare ITO/*l*-ZNRAs/Ti (1.52 μA cm^{-2}) and ITO/*l*-ZNRAs/bare Ti (1.07 μA cm^{-2}). Above results clearly suggest that the face-to-face hybrid ZNRAs-based nanostructure has an enhanced performance of "1 + 1 > 2" in photoelectric conversion. The poor photoelectric properties of single-face ZNRAs nanostructures should be attributed to the generation of great contact resistance between bare planar electrode and ZNRAs. The irregular lengths of nanorods as well as the simple mechanical contact reduce the effective interface area between bare planar electrode and ZNRAs, as shown in Fig. 5(a). By contrast, the face-to-face hybrid nanostructure contains the highly-effective electrode interfaces fabricated by the crystal growing of ZnO nanorods on both electrodes, and the intercrossing of ZnO nanorods enable a fully physical contact of NR-NR, which effectively increase the interfacial contact area and thus a more effective electrical connection.

The schematic diagrams of energy-band structures of the self-powered face-to-face ZNRAs-based UVPDs and its NR-NR junction are displayed in Fig. 6(a) and Fig. 6(b), respectively. Through the crystal growth and rapid annealing, Schottky junction can be formed in the interface of ITO/*n*-ZnO [21,22], and ohmic contact can be realized at the interface of *n*-ZnO/Ti [23]. The extreme surface curvature of the nanorods greatly enhances the surface activity. As a result, the adsorption of oxygen in air takes place on the surface of nanorods where electron depletion regions are created [24,25]. This will results in the bending of energy-band in surface and the formation of extensive NR-

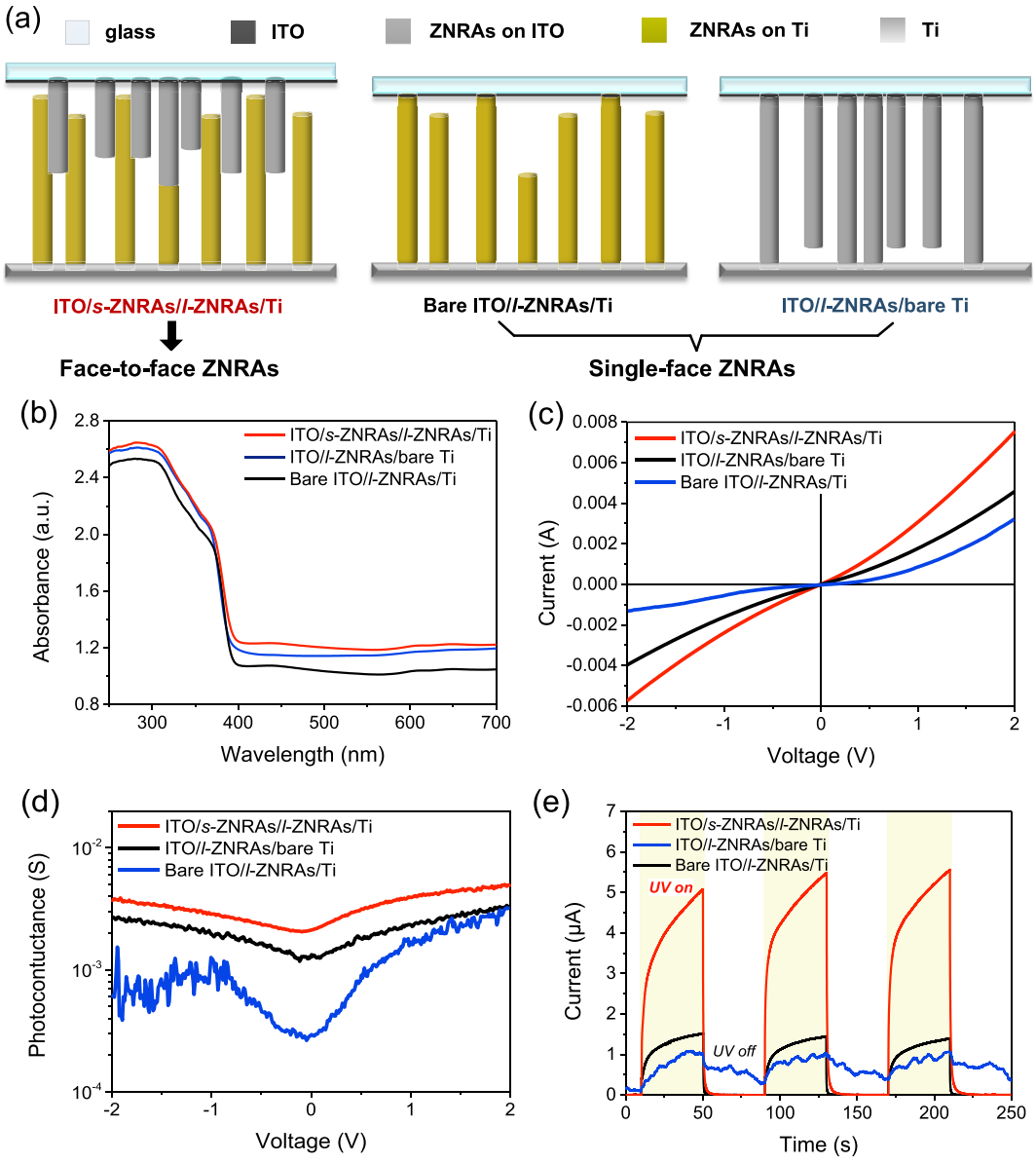

Fig. 5. (a) Schematic structures of the self-powered UVPDs based on face-to-face ITO/*s*-ZNRAs/*l*-ZNRAs/Ti, and single-face bare ITO/*l*-ZNRAs/Ti and ITO/*l*-ZNRAs/bare Ti; (b) Comparison of UV–Vis spectra of above three kinds of devices. Comparisons of (c) *I–V* characteristics and (d) differential conductance of above three kinds of devices under UV irradiation with power density of 2.90 mW cm^{-2}. (e) Time-dependent photoresponses of devices under 3.06 mW cm^{-2} of UV irradiation controlled by switching on/off cycles.

NR homojunctions with the built-in potential vertical to the surface of nanorods. As shown in Fig. 6(b), the symmetrical bending-bands lied at both sides of NR-NR interface enables the holes to migrate to the surface of nanorods and electrons to move to the interior of nanorods. With an UV irradiation, the photo-exited EHPs are separated by built-in potential of ITO/ZnO Schottky junction and NR-NR homojunctions along the directions of length and diameter of the nanorod, respectively. The effective EHP separation in nanorods significantly suppresses the recombination of EHPs. The electrons transport from conductive band (E_C) of ZnO to Ti substrate while the hole transport from valence band (E_V) of ZnO to ITO substrate [26,27]. In this process, the carrier transports have to overcome the NR-NR homojunctions barrier between neighboring nanorods. Thanks to the weak homojunction barrier of NR-NR and the strong built-in potential in Schottky barrier, the carriers can be transported smoothly to electrodes and contribute the generation of photocurrent without applying any external DC voltage to devices.

On account of the presence of Schottky barrier in the ITO/ZnO interface, the face-to-face ZNRAs-based UVPD exhibits a typical rectifying behavior with a turn-on voltage of 1.0 V, as shown in Fig. 6(c). Such a Schottky rectifying characteristic can be described by the thermionic emission-based diode equation [19] as Eq. S(1) and Eq. S(2) in the Supporting Information. With the low-level reversed saturated current and without external voltage, the current transport process can be described as Eq. S(3) and Eq. S(4). Under a 2.90 mW cm^{-2} of UV irradiation, the *I–V* curve is changed to an approximately linear curve. It is suggested that the high free charge densities present during illumination significantly reduce the width of the depletion layer in Schottky junction. As a result, the semiconducting characteristics are transformed to metallic characteristics due to the occurrence of electron tunneling effect. This result is consistent with the other reports [28–31]. Furthermore, a comparison of photovoltaic *I–V* characteristics with and without UV irradiation can be seen in inset of Fig. 6(c). Under UV irradiation, the device exhibits an obvious photovoltaic effect with open-circuit voltage (V_{OC}) of 5.6 mV and short-circuit current (I_{SC}) of 7.2 μAcm^{-2}.

The semi-logarithmic *I–V* curves are shown in Fig. 6(d). According

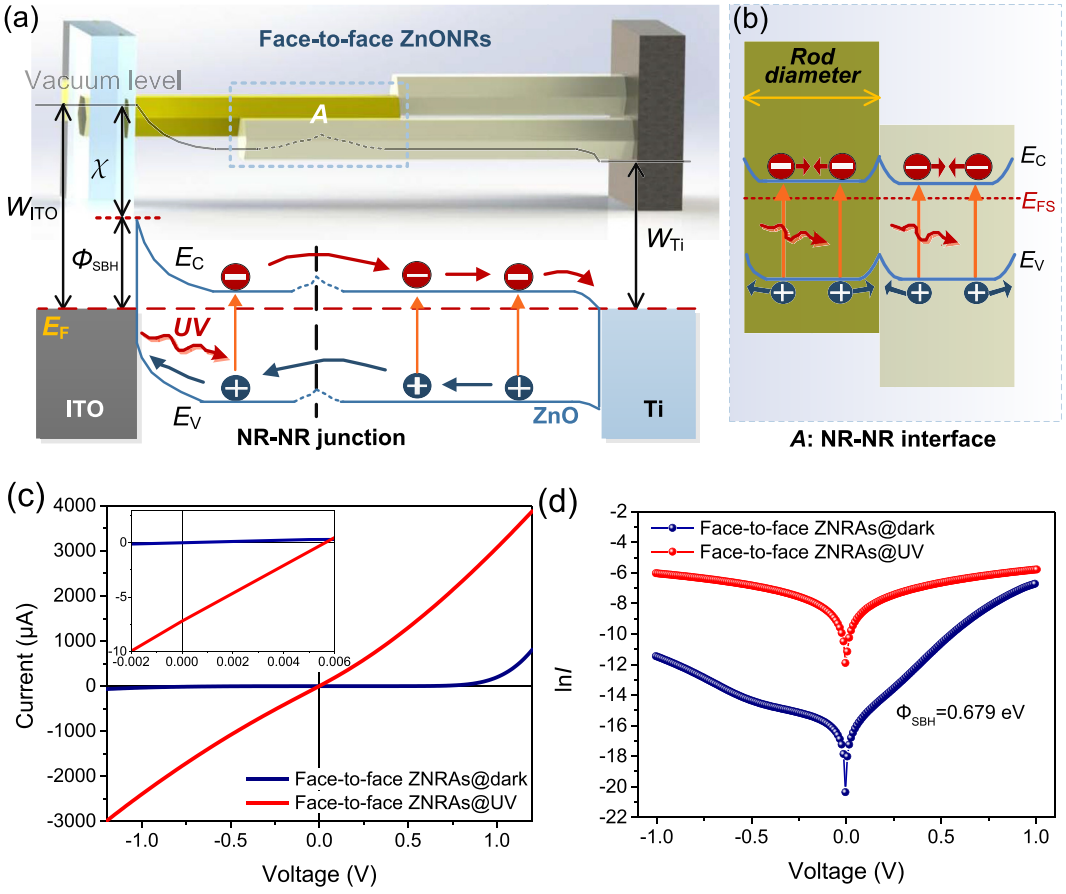

Fig. 6. Schematic diagrams of energy-band structures of (a) the self-powered face-to-face ZNRAs-based UVPDs and (b) its NR-NR junction; Comparison of *I–V* characteristics in (c) linear and (d) semi-logarithmic scale for face-to-face ZNRAs-based UVPDs in dark and under 2.90 mW cm^{-2} of UV irradiation. The inset in (c) is the photovoltaic *I–V* characteristics of the device.

the In*I–V* characteristics, the ideal factor (n) and Schottky barrier height (Φ_{SBH}) are calculated to be 2.285 and 0.679 V, respectively. It is noted that this calculated Φ_{SBH} is slightly higher than the difference between the Fermi level of ITO (E_F = 4.88 V [32]) and the electron affinity of ZnO (χ = 4.25 V [33]). This difference is attributed to the influence of the interface states. It is considered that an interfacial compound layer is formed at ZnO/ITO interface after thermal annealing. These interfacial layer may have a different work function from the ITO layer, which is responsible for the increase of the barrier height [21].

The optimum geometric dimension of ZNRAs plays an important role in the photoresponse performances of face-to-face hybrid ZNRAs-based UVPDs. In order to determine the structure of optimum geometry, the ZNRAs grown on alternative substrates with different nanorod dimensions were designed to pair hybrid each other, e.g. ITO/*s*-ZNRAs/*l*-ZNRAs/Ti, ITO/*l*-ZNRAs/*l*-ZNRAs/Ti and ITO/*l*-ZNRAs/*s*-ZNRAs/Ti, as schematically shown in Fig. 7(a). Fig. 7(b) shows a comparison of UV–Vis absorption spectra of above three kinds of devices. There is no significant difference for three kinds of devices in UV absorption. However, the ITO/*s*-ZNRAs/*l*-ZNRAs/Ti device shows the largest curve slope and thus the best *I–V* response under UV irradiation, as shown in Fig. 7(c). Moreover, the differential conductance spectra in Fig. 7(d) and the time-dependent photoresponse characteristics in Fig. 7(e) demonstrate the hybrid structures of ITO/*s*-ZNRAs/*l*-ZNRAs/Ti and ITO/*l*-ZNRAs/*l*-ZNRAs/Ti with the highest photo-conductance (2.12×10^{-3} S) and the highest photoresponse level (6.6×10^5 on/off current ratio), respectively. Furthermore, the performance of hybrid ITO/*l*-ZNRAs/*l*-ZNRAs/Ti device is clearly better than that of hybrid ITO/*l*-ZNRAs/*s*-ZNRAs/Ti device, which indicates that the length of ZnO nanorod-nanorod (NR-NR) homojunction is an important factor in performance enhancement of devices.

To gain more insights into the effects of geometric dimension of ZNRAs on the photoelectric properties of face-to-face hybrid ZNRAs-based UVPDs, the transport behaviors of photo-excited carriers in the hybrid nanostructure should be considered. In a face-to-face hybrid ZNRAs-based UVPDs, photo-excited EHPs are separated by built-in potential in the depletion region of ITO/ZnO Schottky junction to generate photocurrent, as shown in Fig. 6(a) in front. The depletion region width (W) of ITO/ZnO Schottky junction can be calculated by:

$$W = \sqrt{\frac{2\varepsilon_S(\Phi_{SBH} - V)}{eN_D}}, \quad (1)$$

$$\varepsilon_S = \varepsilon_{r-ZnO}\varepsilon_0, \quad (2)$$

where ε_S is semiconductor permittivity, $\varepsilon_{r\text{-}ZnO}$ is ZnO relative permittivity (8.66 at 300 K [34]), ε_0 is the vacuum permittivity, and N_D is carrier concentration (2.1×10^{15} cm^{-3} for wurtzitic ZnO grown by hydrothermal method [35]). The effective W of ITO/ZnO Schottky junction is less than 1 μm (calculated to be ~5.6×10^{-1} μm). In order to achieve the maximum photoresponse, the optimum length of ZnO nanorod in ITO/ZnO junction should be limited to $l_{ZnO} = W + L_p \leq 1.0$ μm, where L_p is the minority carrier diffusion length. Furthermore, the extensive NR-NR homojunctions are suggested to play an important role in light absorption and photoelectric conversion. Two requirements must be met for achieve the maximum photoelectric conversion: 1) The intercrossed length among nanoroads determines the extent of NR-NR homojunctions. The extensive NR-NR homojunctions can fully harvest and absorb the UV light energy; 2) The NR-NR homojunctions should get as close as possible to the depletion region of ITO/ZnO Schottky junction to separate the photo-excited EHPs. According to above

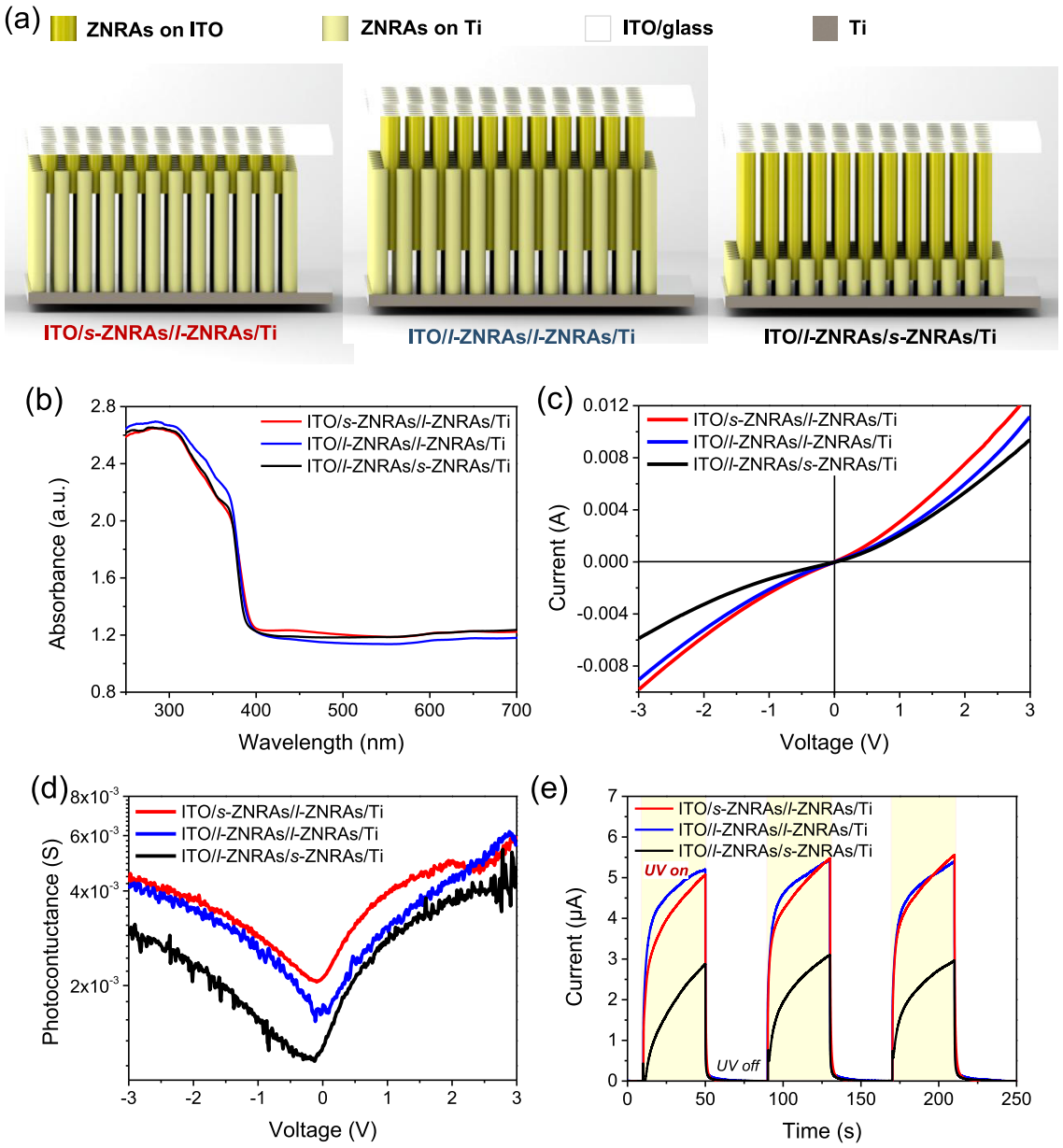

Fig. 7. (a) Schematic structures of the self-powered UVPDs based on face-to-face ITO/*s*-ZNRAs/*l*-ZNRAs/Ti, ITO/*l*-ZNRAs/*l*-ZNRAs/Ti and ITO/*l*-ZNRAs/*s*-ZNRAs/Ti structure; (b) Comparison of UV–Vis spectra of above three kinds of UVPDs; Comparisons of (c) *I–V* characteristics and (d) differential conductance of above three kinds of devices under UV irradiation with power density of 2.90 mW cm^{-2}. (e) Time-dependent photoresponses of devices under 3.06 mW cm^{-2} of UV irradiation controlled by switching on/off cycles.

requirements, the device design based on the hybrid of two short ZNRAs structures is firstly excluded from candidates because the hybrid length of NR-NR is too short to absorb the UV light fully, as illustrated in Fig. 8(a). Meanwhile, the ITO/*l*-ZNRAs/*s*-ZNRAs/Ti structure is not an optimum candidate because the short NR-NR homojunction is far from the depletion region of ITO/ZnO Schottky junction, as show in Fig. 8(b). By contrast, the NR-NR homojunctions in ITO/*s*-ZNRAs/*l*-ZNRAs/Ti structure are closed to the depletion region of ITO/ZnO Schottky junction. However, its photoresponse performance is affected by a trade-off between the low separation efficiency of EHPs due to the limited NR-NR homojunctions and the excellent photo-conductance (see Fig. 7(d)) induced by the short carrier transport length, as shown in Fig. 8(c). The ITO/*l*-ZNRAs/*l*-ZNRAs/Ti structure is considered to be optimum hybrid structure due to the extensive NR-NR homojunctions that are close to ITO windows, as shown in Fig. 8(d). However, its photoresponse property is not significantly improved in comparison with the ITO/*s*-ZNRAs/*l*-ZNRAs/Ti structure (see Fig. 7(e)), which can be attributed to the long carrier transport length that enables a relative weak photo-conductance.

The responsivity (R_s) and specific detectivity (D^*) of the optimum UVPD based on ITO/*l*-ZNRAs/*l*-ZNRAs/Ti structure were further investigated. R_s is defined as:

$$R_s = \frac{I_{ph}}{SP_{opt}}, \tag{6}$$

where I_{ph} is the photocurrent under the UV irradiation, S is the device area and P_{opt} is the specific UV intensity upon the active region of the devices. D^* can be used to determine how weak the light signal could be identified from the noise environment. Assuming that shot noise from the dark current will mainly contribute to the total noise, the detectivity can be evaluated by:

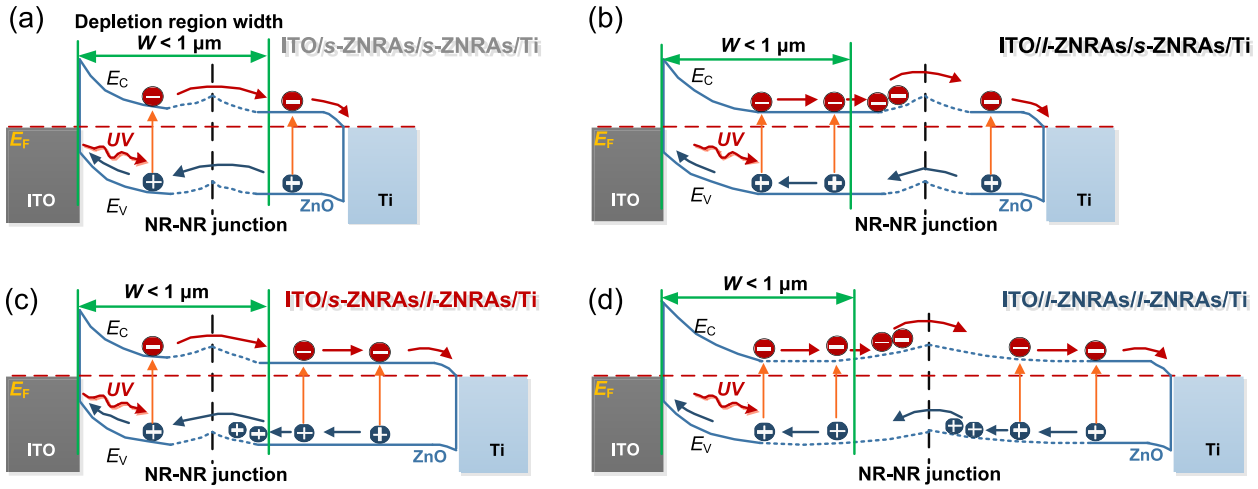

Fig. 8. Schematic energy band diagrams and the mechanisms of carrier transport of the face-to-face hybrid ZNRAs devices based on (a) ITO/*s*-ZNRAs/*s*-ZNRAs/Ti, (b) ITO/*l*-ZNRAs/*s*-ZNRAs/Ti, (c) ITO/*s*-ZNRAs/*l*-ZNRAs/Ti and (d) ITO/*l*-ZNRAs/*l*-ZNRAs/Ti structures.

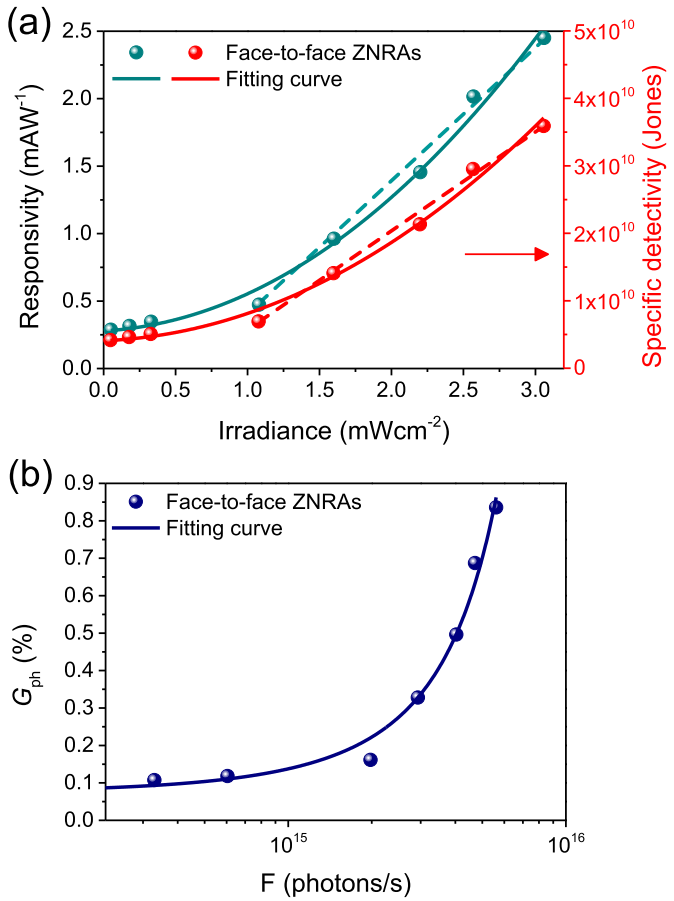

Fig. 9. (a) UV intensity dependence of responsivity and specific detectivity of the optimum UVPD based on ITO/*l*-ZNRAs/*l*-ZNRAs/Ti structure; (b) Photon absorption rate dependence of photoconductive gain of the device.

$$D^* = \frac{J_{ph}\sqrt{S}}{P_{opt}\sqrt{2eI_d}}, \quad (7)$$

J_{ph} is photocurrent density and I_d is dark current. Fig. 9(a) shows the UV intensity dependence of responsivity and specific detectivity of the optimum UVPD without external bias. The R_s is nearly proportional to the UV intensity with power range from 1.08–3.06 mW cm^{-2}, and the device exhibits a R_s of around 2.45 mA W^{-1} for the UV intensity of 3.06 mW cm^{-2}, which is much larger than that of previous report [18,36]. Such high responsivity should be attributed to the long lifetime of the photo-excited carrier, induced by combination influence of ITO/ZnO Schottky junction and NR-NR homojunction on the effective suppression of EHPs recombination. Furthermore, it is noticeable from

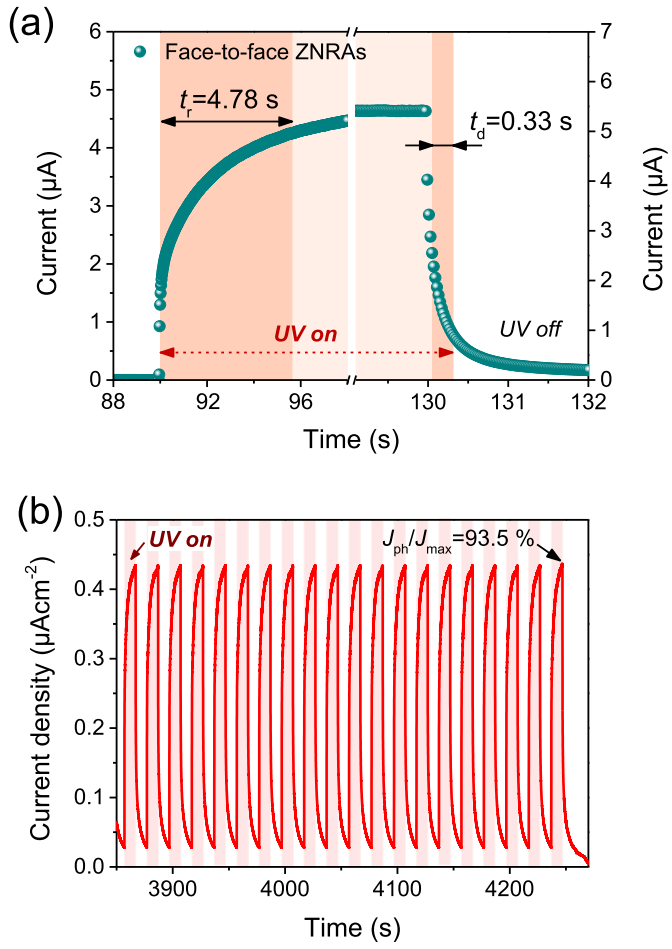

Fig. 10. (a) Rise-time and fall-time measurements of the optimum self-powered UVPD based on ITO/*l*-ZNRAs/*l*-ZNRAs/Ti structure; (b) On/off cyclic photoresponse of the optimum self-powered UVPDs under a 0.05 Hz and 1.08 mW cm^{-2} of UV irradiation, which is extracted from the tail of a 4250-s cyclic test.

Table 1
Comparison of characteristic parameters of current study and the relevant literature.

Device	Method	Responsivity ($mA \cdot W^{-1}$)	On/off ratio	Rise time (s)	Decay time (s)	Cyclic balance (%)	Ref.
Ag-doped ZnO nanofibers	Electrospin	1.28	2.5×10^4	3.9	4.7	–	[36]
Ga_2O_3/ZnO microwire	Chemical vapor deposition	9.7	$\sim 10^3$	10^{-4}	9×10^{-4}	–	[7]
Se/ZnO	Hydrothermal/chemical vapor deposition	2.65	10^4	6.9×10^{-4}	1.4×10^{-2}	–	[3]
Graphene/ZnO nanowires	Chemical vapor deposition/thermal evaporation	5.15×10^{-3}	–	3	0.47	–	[18]
Pt/Al_2O_3/ZnO NRAs	Atomic layer deposition/hydrothermal	6.53×10^{-4}	7.28	< 1	< 1	–	[28]
Reduced graphene oxide/ZnO nanoparticles	Solvothermal	20 nA (80 mW•cm^{-2})	430	< 0.2	< 0.2	–	[42]
CdS/ZnO nanowire arrays (liquid)	Lithography/dipcoating/hydrothermal	35.4	1875	0.18	0.32	42 (~300 cycles)	[12]
Cu nanowires/ZnO film	Spincoating	70 pA (0.8 mW•cm^{-2})	~35	> 12.48	> 10.7	–	[43]
Sb-doped ZnO nanowires	Chemical vapor deposition	23 nA	22	0.1	0.1	–	[30]
Face-to-face ZnO NRAs	Hydrothermal	2.45	6.6×10^5	4.78	0.33	93.5 (212 cycles)	Present work

Fig. 9(a) that the optimum UVPD exhibits a high detectivity of 4.17×10^9 Jones (Jones = $cm \cdot Hz^{1/2} W^{-1}$) under a low UV irradiation of 50 μW cm^{-2}. The high detectivity for a low UV intensity can be attributed to the strong photo-absorption and photoelectric conversion capacities of the 3-D intercrossed ZNRAs nanostructure.

Photoconductive gain (G_{ph}) is used to further assess photoelectric conversion efficiency of the optimum UVPD. G_{ph} is defined as the number of electrons collected by electrodes under one incident photon, which is defined as:

$$G_{ph} = \frac{I_{ph}}{P_{opt}} \times \frac{h\nu}{e} = \frac{I_{ph}}{e} \times \frac{1}{F}, \tag{8}$$

where $h\nu$ is the energy of the incident photon, and F is the photon absorption rate. It can be seen from Fig. 9(b) that the optimum UVPD displays an exponential increase in G_{ph} with the increase of photon absorption rate, and G_{ph} present a fast increase in high F, up to 0.84% at photon absorption rate of 5.6×10^{15} s^{-1}, rather than a decrease as reported in other research [37,38]. This good photoelectric behavior can be also explained by the effective built-in potential in the hybrid nanostructure, which results in an extremely low carrier recombination even at high incident power. On the other hand, it may be due to the fact that the self-powered devices were measured without applying any external DC voltage. This means that the recombination of EHPs in these devices are higher than that of devices with external DC voltage, thereby resulting in the increase of the responsivity and detectivity when increasing the incident light intensity.

The time-domain photoresponse characteristics of the optimum self-powered UVPD based on ITO/*l*-ZNRAs/*l*-ZNRAs/Ti structure were further investigated. As shown in Fig. 10 (a), the optimum UVPD exhibits a rise-time (t_r) of 4.78 s and a fall-time (t_d) of 0.33 s. The chemisorption and photo-desorption of oxygen could be responsible for the different photoresponse behaviors [25,39,40].

Furthermore, the stability of the photodetector was investigated by an on/off cyclic photoresponse tests. Fig. 10(b) shows 20 cycles of on/off cyclic photoresponse of the optimum UVPD under a 0.05 Hz and 1.08 mW cm^{-2} of UV irradiation, which is extracted from the tail of a 4250-s cyclic test. The device exhibits uniform and repeatable photoresponse with a high on/off current ratio of 6.4×10^5 and relative balance ($I_{ph}/I_{max} \times 100\%$) as high as ~ 93.5% after over 4250 s test. This excellent reproducibility and stability shown in cyclic photoresponse test implies a potential application in photosensing and optical communication.

When compared with the ZnO-based UVPDs with applying external DC voltage, e.g. Ref. [41], the relative low photoresponse in our devices is due to the fact that the devices were measured without applying any external DC voltage to the devices. In our previous work [25], it has been demonstrated that the external bias can promote the improvement of photoresponse of ZnO-based UVPDs. Table 1 presents a comparison of characteristic parameters of current study and the reported works related with ZnO-based self-powered UVPDs without applying external DC voltage.

4. Conclusion

In summary, we report a self-powered UVPDs based on the face-to-face hybrid ZNRAs nanostructure. Large-area free-standing ZNRAs were prepared on ITO and Ti substrates using a facile hydrothermal method, and the well crystal quality and the vertical orientation to the substrate have been verified by the measurements of SEM and XRD. Different geometric dimension of ZNRAs/ITO and ZNRAs/Ti structures were designed to pair hybrid each other for achieving the optimum photoelectric performance. Experimentally, it was found that the optimum UVPD based on face-to-face hybrid ITO/*l*-ZNRAs/*l*-ZNRAs/Ti structure exhibits '1 + 1 > 2' enhancement in photoelectric conversion without external power source when compared with single-face ZNRAs-based

UVPDs, and the optimum UVPD demonstrates a responsivity of 2.45 mA W^{-1} and on/off current ratio of 6.6×10^5 under a UV irradiation of 3.06 μW cm^{-2} as well as a high durability with a cyclic balance of no less than 93.5% in a 4250 s of on/off irradiation. Owing to the Schottky junctions in ITO/ZnO interface as well as the formation of extensive ZnO NR-NR homojunction, the photo-exited EHPs are separated by two effective built-in potential significantly decrease the recombination of EHPs. All of these results indicate that this novel self-powered UVPD can be a promising candidate as a low-cost UVPD for a potential application in photosensing and optical communication.

Photographs of the photodetectors based on face-to-face ZNRAs; SEM images of different face-to-face ZNRAs; Calculation of Schottky barrier height in face-to-face ZNRAs-based UVPDs.

Acknowledgment

This work was supported by the National Natural Science Foundation of China (Grant No. 61574117 and 61574119), the Natural Science Foundation of Guangdong Province (Grant No. 2018B030311002) and the China Scholarship Council (Grant No. 201806310044).

Appendix A. Supplementary data

Supplementary data to this article can be found online at https://doi.org/10.1016/j.nanoen.2019.104042.

Conflicts of interest

There are no conflicts to declare.

References

[1] Y. Wang, L. Zhu, Y. Feng, Z. Wang, Z.L. Wang, Adv. Funct. Mater. 29 (2019) 1807111.
[2] M. Chen, B. Zhao, G. Hu, X. Fang, H. Wang, L. Wang, J. Luo, X. Han, X. Wang, C. Pan, Z.L. Wang, Adv. Funct. Mater. 28 (2018) 1706379.
[3] K. Hu, F. Teng, L. Zheng, P. Yu, Z. Zhang, H. Chen, X. Fang, Laser Photonics Rev. 11 (2017) 1600257.
[4] C.-H. Lin, H.-C. Fu, D.-H. Lien, C.-Y. Hsu, J.-H. He, Nano Energy 51 (2018) 294–299.
[5] Z.L. Wang, Nano Energy 54 (2018) 477–483.
[6] D. Xiang, C. Han, Z. Hu, B. Lei, Y. Liu, L. Wang, W.P. Hu, W. Chen, Small 11 (2015) 4829–4836.
[7] B. Zhao, F. Wang, H. Chen, L. Zheng, L. Su, D. Zhao, X. Fang, Adv. Funct. Mater. 27 (2017) 1700264.
[8] Z. Zhang, Y. Ning, X. Fang, J. Mater. Chem. C 7 (2019) 223–229.
[9] D. You, C. Xu, W. Zhang, J. Zhao, F. Qin, Z. Shi, Nano Energy 62 (2019) 310–318.
[10] P. Samadipakchin, H.R. Mortaheb, A. Zolfaghari, J. Photochem. Photobiol. A Chem. 337 (2017) 91–99.
[11] H. Zhang, A.V. Babichev, G. Jacopin, P. Lavenus, F.H. Julien, A. Yu. Egorov, J. Zhang, T. Pauporté, M. Tchernycheva, J. Appl. Phys. 114 (2013) 234505.
[12] Z. Bai, M. Fu, Y. Zhang, J. Mater. Sci. 52 (2017) 1308–1317.
[13] X.-W. Fu, Z.-M. Liao, Y.-B. Zhou, H.-C. Wu, Y.-Q. Bie, J. Xu, D.-P. Yu, Appl. Phys. Lett. 100 (2012) 223114.
[14] V.Q. Dang, T.Q. Trung, D.I. Kim, T. Duy le, B.U. Hwang, D.W. Lee, B.Y. Kim, D. Toan le, N.E. Lee, Small 11 (2015) 3054–3065.
[15] Z.L. Wang, J. Song, Science 312 (2006) 242–246.
[16] Y.D. Park, J.A. Lim, H.S. Lee, K. Cho, Mater. Today 10 (2007) 46–54.
[17] S. Chen, L. Wang, R. Shao, J. Zou, R. Cai, J. Lin, C. Zhu, J. Zhang, F. Xu, J. Cao, J. Feng, J. Qi, P. Gao, Nano Energy 48 (2018) 560–568.
[18] B.D. Boruah, A. Mukherjee, A. Misra, Nanotechnology 27 (2016) 095205.
[19] D. Li, F. He, T. Ye, B. Sun, J. Fan, X. Yu, N. Lei, Z. Yan, Y. Chen, W. Zhang, ACS Appl. Mater. Interfaces 9 (2017) 8161–8168.
[20] D. Guo, H. Shi, Y. Qian, M. Lv, P. Li, Y. Su, Q. Liu, K. Chen, S. Wang, C. Cui, Semicond. Sci. Technol. 32 (2017) 03LT01.
[21] J.K. Sheu, Y.K. Su, G.C. Chi, M.J. Jou, C.M. Chang, Appl. Phys. Lett. 72 (1998) 3317–3319.
[22] N. Biyikli, I. Kimukin, T. Kartaloglu, O. Aytur, E. Ozbay, Appl. Phys. Lett. 82 (2003) 2344–2346.
[23] A. Jarjour, J.W. Cox, W.T. Ruane, H. Von Wenckstern, M. Grundmann, L.J. Brillson, Ann. Phys. 530 (2018) 1700335.
[24] H. Xu, W. Fan, A. Rosa, R. Zhang, T. Frauenheim, Phys. Rev. B 79 (2009) 073402.
[25] C. Chen, S. Zhang, B. Hu, H. San, Z. Cheng, W. Hofmann, Composites Part B 164 (2019) 640–647.
[26] L. Hu, L. Wu, M. Liao, X. Fang, Adv. Mater. 23 (2011) 1988–1992.
[27] M. Chen, L. Hu, J. Xu, M. Liao, L. Wu, X. Fang, Small 7 (2011) 2449–2453.
[28] Z. Zhang, Q. Liao, Y. Yu, X. Wang, Y. Zhang, Nano Energy 9 (2014) 237–244.
[29] Y.Q. Bie, Z.M. Liao, H.Z. Zhang, G.R. Li, Y. Ye, Y.B. Zhou, J. Xu, Z.X. Qin, L. Dai, D.P. Yu, Adv. Mater. 23 (2011) 649–653.
[30] Y. Yang, W. Guo, J. Qi, J. Zhao, Y. Zhang, Appl. Phys. Lett. 97 (2010) 223113.
[31] Y. Jin, J. Wang, B. Sun, J.C. Blakesley, N.C. Greenham, Nano Lett. 8 (2008) 1649–1653.
[32] V. Nalla, L. Polavarapu, K.K. Manga, B.M. Goh, K.P. Loh, Q.H. Xu, W. Ji, Nanotechnology 21 (2010) 415203.
[33] M.W. Allen, S.M. Durbin, Phys. Rev. B 82 (2010) 1462–1465.
[34] Y. Yang, W. Guo, X. Wang, Z. Wang, J. Qi, Y. Zhang, Nano Lett. 12 (2012) 1919–1922.
[35] M. Allen, S. Durbin, J. Metson, Appl. Phys. Lett. 91 (2007) 053512.
[36] Y. Ning, Z. Zhang, F. Teng, X. Fang, Small 14 (2018) 1703754.
[37] C. Soci, A. Zhang, B. Xiang, S.A. Dayeh, D.P.R. Aplin, J. Park, X.Y. Bao, Y.H. Lo, D. Wang, Nano Lett. 7 (2007) 1003–1009.
[38] V.Q. Dang, T.Q. Trung, T. Duy le, B.Y. Kim, S. Siddiqui, W. Lee, N.E. Lee, ACS Appl. Mater. Interfaces 7 (2015) 11032–11040.
[39] J. Cheng, Y. Zhang, R. Guo, J. Cryst. Growth 310 (2008) 57–61.
[40] Y. Takahashi, M. Kanamori, A. Kondoh, H. Minoura, Y. Ohya, Jpn. J. Appl. Phys. 33 (2014) 6611–6615.
[41] G. Cheng, X. Wu, B. Liu, B. Li, X. Zhang, Z. Du, Appl. Phys. Lett. 99 (2011) 203105.
[42] Z. Zhan, L. Zheng, Y. Pan, G. Sun, L. Li, J. Mater. Chem. 22 (2012) 2589–2595.
[43] F. Teng, L. Zheng, K. Hu, H. Chen, Y. Li, Z. Zhang, X. Fang, J. Mater. Chem. C 4 (2016) 8416–8421.

Changsong Chen is currently pursuing the Ph.D. degree in Microelectronics and Solid State Electronics from Pen-Tung Sah Institute of Micro-Nano Science and Technology, Xiamen University. He received his B.E. degree in Measurement & Control Technology and Instrumentations from Jilin University in 2014. His research interests are in the fields of energy-conversion devices and systems based on nanostructured semiconductors.

Baofa Hu received his B.S. degree in School of Physics and Electronics from Hunan University in 2007 and obtained his master degree in Department of Electronic Engineering from Xiamen University in 2013. He is currently completing a Ph.D. in Measuring and Testing Technologies and Instruments at Dr. Haisheng San's group in Xiamen University. His research interests are focused on wireless-sensor, MEMS and micro-energy.

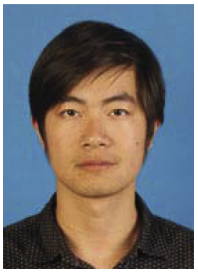

Zhen Wang received his bachelor degree in Materials chemistry at Lanzhou University in 2017. He currently is a master candidate in Microelectronics and Solid State Electronics in Dr. Haisheng San's group at Xiamen University. His research interests include experimental and theoretical research: the growth of one-dimensional nano-materials, ultraviolet detector and micro-energy.

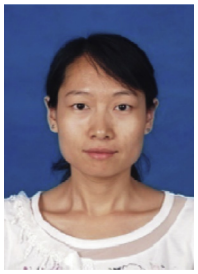

Xueqin Lv is an associate professor in Pen-Tung Sah Institute of Micro-Nano Science and Technology, Xiamen University. She received her Ph.D degree in Microelectronics and Solid State Electronics from Institute of Semiconductor, Chinese Academy of Sciences (CAS), in 2010. Her research interests are in preparation and characterization of semiconductor optoelectronic materials, development, performance characterization and application of grating external cavity semiconductor laser.

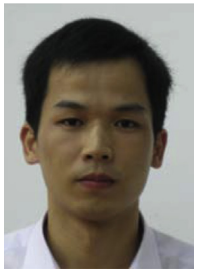

Chunquan Zhang is an engineer in Pen-Tung Sah Institute of Micro-Nano Science and Technology, Xiamen University. He studied in Xiamen University from 2004 to 2008, and obtained a bachelor's degree. Since his graduation, he has been engaged in the development and research of semiconductor devices and sensor technology.

Binbin Chen is an engineer in Pen-Tung Sah Institute of Micro-Nano Science and Technology, Xiamen University. She studied in Xiamen Staff and Workers University from 2004 to 2007, with a junior college degree. Since her graduation, she has been engaged in the development and research of semiconductor devices and sensor technology.

Haisheng San received the B.Sc. degree in mechanical engineering from Southwest University of Science and Technology, Mianyang, China, in 1993. He received the Ph.D degree in material physics and chemistry from Lanzhou University, Lanzhou, China, in 2006. During 2003 to 2006, he was involved in the study of high-speed optoelectronic devices in Institute of Semiconductor, Chinese Academy of Sciences (CAS), Beijing, China. Presently, he is a Full Professor in Pen-Tung Sah Institute of Micro-Nano Science and Technology, Xiamen University, Xiamen, China. His research interests are in modeling, fabrication, and characterization of MEMS and NEMS devices and sensors and power-MEMS

Werner Hofmann is a professor in Institute of Solid State Physics, Technische Universität Berlin. He received his Ph.D. degree in Walter Schottky Institute, Technische Universität München, in 2009. From 2010 to 2013, he worked as a postdoctoral fellow in Department of Electrical Engineering and Computer Sciences, University of California, Berkeley. His research interests mainly focus on modeling and fabrication of high-speed vertical-cavity surface-emitting lasers (VCSEL).